Synergy of Active and Passive Airborne Thermal Infrared Systems for Surface Compositional Mapping.

Simon J. Hook', Thomas J. Cudahy[2], Anne B. Kahle[1] and Lewis B. Whitboum[2]

1. Jet Propulsion Laboratory, California Institute of Technology, Pasadena, CA, USA, 91109

2. Commonwealth Scientific Industrial Research Organisation, North Ryde, NSW, Australia 2113

Abstract

NASA Thermal Infrared Multispectral Scanner (TIMS) and CSIRO Mid Infrared Airborne CO_2 Laser Spectrometer (MIRACO_2LAS) data were acquired over the Mount Fitton area, South Australia, in order to evaluate their combined use for geological mapping and mineral exploration. TIMS is a passive, imaging system with six spectral bands in the thermal infrared wavelength region (8- 12 μm) whereas MIRACO_2LAS is an active, profiling system with approximately 100 spectral bands in the 9-11 μm spectral range.

The TIMS and CO_2 laser data were processed to enhance spectral information related to the surface composition (emissivity for TIMS and reflectance for MIRACO_2LAS). This spectral information was compared with existing geological maps and field emissivity spectra, Known geological units were well discriminated in the TIMS imagery, including a range of quartz-rich and carbonate-rich sedimentary units, as well as several unmapped areas of alteration in the

carbonates. However, the limited spectral resolution of TIMS inhibited precise mineralogical identification, In contrast, the high spectral resolution MIRAC0,LAS data provided diagnostic spectral information about a range of minerals including quartz, dolomite, talc and tremolite, albeit along discrete profiles. The widths of some of these diagnostic spectral features were less than 0.2 μm wide, which is much smaller than the resolution of the TIMS bandpasses. The MIRACO$_2$LAS spectra agreed well with spectra of field samples measured by both a field emission spectrometer and a laboratory laser spectrometer. Pure mineral spectra measured by the (bidirectional) laboratory laser spectrometer also agreed well those measured by a conventional laboratory spectrometer measuring directional hemispherical reflectance.

These results indicate that future remote thermal infrared systems designed for improved geological mapping and mineral exploration should incorporate both an imager for mapping lithological units, and a high spectral resolution profiler for mineral identification.

Introduction

The radiation emitted from a surface in the thermal infrared (8-12 pm) is a function of its temperature and emissivity. Most geological studies, are less concerned with temperature and more concerned with emissivity variations, which are related to variations in the composition of the surface and can provide a means for remote geological mapping. In order to evaluate the use of emissivity variations for geological mapping studies, NASA developed the Thermal Infrared Multispectral Scanner (TIMS). The instrument was first flown in 1982 and since then numerous studies have successfully demonstrated the use of TIMS for geological mapping, (for example,

Kahle and Goetz, 1983; Gillespie *et al.* 1984; Watson, 1985; Lang et *al.* 1987; Lahren *et al. 1988;* Abrams et *al.* 1991; Hook et *al.* 1992; Sabine and Realmuto, 1994; Hook et *al.* 1994; Crowley and Hook; 1996, Watson et al. 1996). TIMS is a passive instrument measuring naturally emitted surface radiation in six bands between 8 and 12 pm. Passive instruments are presently limited to broad spectral bandwidths in order to obtain an adequate signal-to-noise ratio. In addition, the data acquired by passive instruments are influenced by uncertainties introduced by the presence of atmospheric gases, and the strong dependence of emission on temperature. As a result, TIMS data are used to *discriminate* different rock types rather than to *identify* rock types based on the presence of one or more emission features.

Around the time of the first TIMS flights, Kahle *et al. (1984)* were evaluating an active airborne laser system for mineral identification. This active system measured reflectance of the surface in the thermal infrared, reflectance spectra being the complement of emissivity spectra (Siegal and Howell, 1982). Active systems have several advantages over passive systems. They include better signal-to-noise ratios allowing narrower bandwidths and the absence of the complicating effects of temperature (Kahle *et al.* 1984) allowing operation under cloudy skies. However, active instruments are more complex than passive instruments and thus far have been limited to profiling instruments. While the instrument used by Kahle *et al. (1984)* only had two channels in the thermal infrared further limiting its usefulness, it demonstrated the potential of active instruments. More recently, Eberhardt *et al. (1988)* examined the possibility of using a high spectral resolution CO_2 laser that tuned through about 100 wavelengths between 9.1 and 11.2 μm. From this, CSIRO Australia then developed the profiling Mid Infrared Airborne CO_2 Laser Spectrometer (MIRACO_2LAS) to investigate the capabilities of high spectral resolution

TIR remote sensing for applications in mineral mapping (Whitbourn *et al.* 1990, 1991, 1994, Hausknecht *et al.* 1993, Cudahy *et al.* 1994A).

An instrument with both an active, high spectral resolution profiler and a passive, broad band imager should prove useful for geological studies since the profile data could be used to identify the mineralogy of a given lithological unit whereas the imager could be used to map its surface distribution. In order to investigate this possibility the NASA TIMS was shipped to Australia in 1993 and flown with the CSIRO MIRAC0$_2$LAS on an F-27 aircraft. Several sites were flown in Australia and this study reports on the data acquired over the Mount Fitton area in the Flinders Ranges, South Australia,

Theoretical Framework

The reflectance and emissivity spectra of minerals exhibit diagnostic features at various wavelengths which provide a means for their remote discrimination and identification. These features are produced by electronic or vibrational processes resulting from the interaction of electromagnetic energy with the atoms and molecules which comprise the minerals that make up a rock. These different processes require varying amounts of energy to proceed, and therefore are manifested in different wavelength regions. Electronic processes require the most energy and result in spectral features in the visible and near-infrared wavelength regions. Fundamental vibrational processes require less energy and evidence for them occurs in the infrared beyond 2.5 μm. Between 0.5 and 2.5 μm there is an overlap of features due to electronic processes and the excitation of overtone and combination-tone vibrations (Hunt, 1980). Of particular interest to

geological studies are the emission minimum associated with the Si-O bond in the thermal infrared (8- 12 μm). This feature is commonly referred to as the reststrahlen feature. This restrahlen feature occurs at relatively short wavelengths (8.5 pm) for framework silicates (quartz, feldspar) and at progressively longer wavelengths for silicates having sheet, chain and isolated SiO_4 tetrahedral (Hunt, 1980).

Reflectance spectra converted to emissivity for a variety of pure minerals that occur in the study area are shown in Figure 1. The reflectance data were converted to emissivity using the simplest form of Kirchhoff's Law (E= 1-R). The spectra are displayed in terms of emissivity to allow them to be easily used in conjunction with the emissivity imagery displayed later. The spectra shown in the left panel of Figure 1 were measured with the Jet Propulsion Laboratory Nicolet Model 520 Interferometer Spectrometer. The spectra have a resolution of 4 wavenumbers and were measured in the directional hemispherical reflectance mode. The spectra shown in the right panel of Figure 1 were measured with a laboratory version of MIRAC0LAS, which is described in a subsequent section. It should be noted that the laser measurements are hi-directional and, depending on the scattering cross section of the material being measured, may not be directly related to directional hemispherical reflectance by the simple form of Kirchhoff's Law that we have used here. The laboratory $C0_2$ laser spectrometer does not measure the reflectance at even increments across the wavelength range, because the reflectance is measured at the wavelengths of specific CO_2 lines. Crosses in Figure 1 mark the positions of these lines. In addition, the CO_2 laser only covers the wavelength range from 9.1 to 11.2 μm. Nonetheless, within that range, the data from the two instruments are in good agreement. The shift of the reststrahlen feature from shorter to longer wavelengths with the change in the Si-O bonding of the silicate minerals is also

apparent, The carbonate minerals show a feature around 11 μm which migrates to longer wavelengths as the atomic weight of the cation increases (Liese, 1975; Lyon and Green, 1975; van der Marel and Beutelspacher, 1976). As a result the dolomite minimum is at slight] y longer wavelengths than the magnesite minimum.

TIMS System and Data Processing

The TIMS has six channels between 8 and 12 pm, an instantaneous field of view of 2.5 milliradians and a total field of view of 76.56°. The central positions of the six TIMS channels in micrometers were: 8.353, 8.740, 9.134, 9.832, 10.687 and 11.599. The TIMS data were acquired from an altitude of 1220 m on June 17th 1993 under clear skies. There are 750 pixels in a TIMS scanline and, after correction for panoramic distortion, each pixel is 4 x 4 m in size. However, the TIMS instrument could not be mounted sufficiently close to the skin of the Australian F-27 aircraft to avoid the edges of the scan partially imaging the inside of the viewing port, As a result there is some darkening on the edges of the image. Initially the TIMS data were calibrated to radiance at the sensor (Palluconi and Meeks, 1985). The atmospheric component to the total radiance was then removed using the MODTRAN radiative transfer model (Berk et al. 1989). MODTRAN derives values for the atmospheric correction based on an input atmospheric profile, which may be obtained from default profiles in MODTRAN, or the profile may be modified or replaced with local atmospheric data. No local atmospheric values were available and so the default mid-latitude winter profile was used. In order to assess the atmospheric correction the brightness temperature spectrum of an area of dense vegetation was examined. Vegetation has a relatively flat spectral emissivity in the thermal infrared and therefore the

brightness temperatures should be constant. (Brightness temperature is the temperature of the surface calculated with an assumed emissivity of 1.0). The vegetation brightness temperature in five of the six TIMS channels agreed to within 10 C. Channel 1 had a higher temperature than the other channels suggesting incomplete correction for atmospheric water vapor. Therefore the water vapor in the mid-latitude winter profile was reduced until the temperatures derived over the area of vegetation from all six TIMS channels agreed to within 1 degree.

After atmospheric correction, the ground radiance values are a function only of surface temperature and emissivity. In this study we were interested in variations in surface emissivity, because these relate to differences in mineralogy. The emissivity information was extracted using the alpha-residual technique (Hook *et al.* 1992; Kealy and Hook, 1993). The resultant alpha-residual spectra have a shape similar to emissivity spectra; however, the mean of each spectrum is zero. This method was chosen over other methods since emissivity variations can be examined in all six TIMS channels (most other methods force the emissivity to a constant in one channel) and the method is less susceptible to noise than the reference channel and emissivity normalization techniques (Kealy and Hook, 1993).

In addition, the TIMS data were processed with the decorrelation stretch algorithm for display (Soha and Schwartz, 1978; Gillespie *et al.* 1986). This technique causes the spectral differences between surface units to be displayed as color differences, while most of the temperature variation is displayed as intensity differences (Kahle and Goetz, 1983).

CO_2 Laser System and Data Processing

The MIRACO_2LAS system is based on a rapidly tuned CO_2 laser (Eberhardt *et al.* 1988) that tunes through approximately 100 wavelengths between 9.1 and 11,2 μm in a burst of 10-μs duration pulses that lasts 1.6 ms. The 1OO-W laser pulses illuminate a 2 m diameter pixel on the ground from an altitude of 400 m. The system is deployed in an F-27 aircraft, at an airspeed of about 80 ms^{-1}, leading to a forward motion of the illuminated pixel of only 130 mm during the 1.6 ms burst duration. The signal scattered by the ground is collected by a 300-mm aperture F/0.83 Cassegrainian telescope feeding a liquid nitrogen cooled HgCdTe detector. A second detector records the power of pulses leaving the aircraft (Whitbourn *et al.* 1990). The ratio of the heights of corresponding pulses from these detectors is later used to produce uncalibrated terrain reflectance.

MIRAC0_2LAS data were acquired on June 9th, 1993 under cloudy skies. The uncalibrated MIRAC0_2LAS spectra are influenced by altitude (inverse square law), instrument (throughput), atmospheric (principally line absorption) and surface reflectance (i.e. compositional) effects. The altitude dependency of the power reflected by the surface was corrected by using aircraft radar altimeter data. Atmospheric line absorption (alpha-line), which are chiefly related to water vapor, were estimated for each MIRAC0_2LAS run using the median spectrum and a segmented-hull approach based on the observation that the Beer-Lambert law can be approximated by a linear function, intersecting zero absorption at zero altitude, for the range of altitudes involved (300 -600 m). Note that atmospheric continuum absorption was found to have no discernible effect at these low altitudes. The instrument throughput function was estimated using a comparison of responses from MIRAC0_2LAS data collected over a dam, with

laboratory laser measurements of the reflectance of water roughened by an airstream. These corrections are described in detail by Cudahy et *al. (* 1994B).

Field Spectral Measurements

In-situ emissivity data were measured using the JPL micro Fourier Transform Interferometer (μFTIR). The μFTIR is a lightweight, rugged, high spectral resolution interferometer built by Designs and Prototypes and modified by the Jet Propulsion Laboratory (Hook and Kahle, 1996). "The instrument has a spectral resolution of -6 wavenumbers, weighs 16 kg including batteries and computer, and can be operated easily by two people in the field.

Geology of the Mount Fitton Area

A geological map and corresponding TIMS decorrelation stretch image for the study area is shown in Figure 2. The regional geology has been mapped by Coats and Blisset (197 1). The oldest rocks in the area shown are the Proterozoic (Adelaidean) sedimentary rocks of the Umberatana and Wilpena Groups which unconformably overlie the Proterozoic (Carpentarian) Yerila and Terrapinna granites and granite porphyrins. The Umberatana Group in the region includes, in order of decreasing age, the Bolls Bollana, Balcanoona, Amberoona and Mount Curtis Tillite Formations.

The Balcanoona Formation consists of brown weathering pale gray dolomite and lower units of massive to thinly bedded blue-gray algal limestones. The Amberoona Formation consists of

finely laminated green and gray-green siltstones with minor well-bedded sandy limestone. The overlying Mount Curtis Tillite formation consists of massive gray-green dolomitic graywacke, tillite and minor quartzite. In places, this unit may include parts of the Fortress Hill Formation, which is predominantly a gray siltstone. The base of the Wilpena group is marked by the Nuccaleena formation consisting of purple shales and pink weathering dolomite, which passes quickly into the calcareous gray and gray-green siltstones of the Wonoka formation. The area is overlain in places by Quaternary alluvium.

The Balcanoona Formation plays host to shear zone and stratabound talc deposits. The shear-zone deposits occur near the lower contact with the underlying Bolls Bollana tillites whereas the stratabound deposits occur near the upper contact with the Amberoona siltstones. The shear-zone deposits follow the regional E-W foliation and dip 60° to 80° to the south. They are associated with quartz in veins as well as magnesite within thick pods. Tremolite is largely absent from the shear zone deposits, The stratabound talc deposits are much larger than the shear-zone deposits. They are typically associated with tremolite and chert. Magnesite appears to be absent.

Talc was formed by the hydrothermal metasomatic replacement of dolomite along faults, fractures and the regional pattern of schistocity (Coats and Blisset, 197 1). The source of fluids was likely to be the Lower Ordovician Mudnawantana Granite which has its nearest outcrop 10 km to the east. This source for the siliceous fluids is evidenced by the intervening Bolls Bollana tillites also being hydrothermally altered along fracture and bedding planes. Metrological work by Still well and Edwards (1951) suggested that the silica-bearing solutions transformed dolomite to

tremolite where Ca was retained but produced talc where Ca was removed, This often produced a signature of early-formed tremolite that was subsequently replaced by talc. The difference in style between the shear zone and stratabound talc deposits was suggested by Sprigg (195 1) to be related to the behaviour of the relatively incompetent Balcanoona Formation and the enclosing competent Amberoona and Bolls Bollana Formations during folding. Strain was concentrated along the stratigraphic contacts producing zones of weakness and subsequent increased fluid movement, The role of pending of the hydrothermal fluids at the top of the Balcanoona Formation has also been suggested (Powell, *pers. comm.* 1995).

Data Interpretation

Figure 2 shows the decorrelation stretch image and corresponding simplified geological map for the area. In this image, quartz rich areas have red, purple and orange hues and carbonate-rich areas have green and blue hues. The quartzites of the Mount Curtis Tillite appear orange (Figure 2- Location 1), and the chert associated with the talc deposits in the upper part of the Balcanoona Formation (not shown on the regional geological map) also appear orange (Figure 2- Location B). The quartz-rich siltstones of the Mount Curtis Tillite (possibly the Fortress Hill Formation) appear red (Figure 2- Location A) and the siltstones of the Amberoona Formation appear purple (Figure 2- Location C). The carbonates of the Balcanoona Formation appear green (Figure 2- Location D) as do areas of dense vegetation along creek beds. Areas of talc exposed by mining appear as dark blue (Figure 2- Location F). Within the hinge of a parasitic anticline located at the most western part of the exposed the Balcanoona Formation, there is a light blue area (Figure 2- Location G) associated with chlorite altered carbonate and pods of ferruginous gossan.

Extending up to 1 km from the margin of the Balcanoona Formation with the overlying Amberoona there is a subtle bluish hue associated with dolomite mixed primarily with tremolite and lesser proportions of talc and/or chlorite (Figure 2- Location E).

Figure 3a shows selected field spectra of the main geologic units (Figure 2), namely: quartzite and quartz-rich siltstone from the Mount Curtis Tillite (Spectra 1 and 2, respectively); quartz and phyllosilicate-rich siltstone from the Amberoona Formation (Spectrum 3); and talc, tremolitic-dolomite and dolomite from the Balcanoona Formation (Spectra 4,5 and 6, respectively). The quartzite sample (Spectrum 1- Location 1 with orange hue in Figure 2) and the quartz-rich siltstone (Spectrum 2- Location 2 with red hue in Figure 2) both have a well developed low emissivity doublet centered around 8.5 pm. This signature is characteristic of the reststrahlen feature of quartz (Figure 1- Spectrum Qu). The doublet has a superimposed saw-tooth appearance, caused by incomplete atmospheric correction of the field data (Hook and Kahle, 1996). The quartzite is almost pure quartz, which explains the relatively deeper reststrahlen doublet compared with the neighboring siltstones. Spectrum 3 from the Amberoona Formation (Location 3 with purple hue in Figure 2) also shows the diagnostic quartz reststrahlen doublet, although the quartz feature is weaker than in the spectra from the Mount Curtis Tillite Formation. A phyllosilicate feature near 9.5 μm is also apparent.

This variation in the shape and intensity of the quartz reststrahlen feature between these quartz-bearing rock types is also demonstrated in the airborne data. Both the alpha emissivity spectra (Figure 3b) and the MIRACO$_2$LAS reflectance spectra (Figure 3c) show that the most intense quartz signatures are provided by the quartzite (Spectrum 1), followed by the quartz-rich siltstone

(Spectrum 2) and finally the relatively quartz-poor Amberoona siltstone (Spectrum 3), which has the highest emissivities but relatively lower emissivity near 9.8 μm related to more abundant phyllosilicates (mica and/or clay).

The three field FTIR spectra shown from the carbonate-rich Balcanoona Formation are from samples of talc, a mixture of tremolite and dolomite, and dolomite (Figure 3a - Spectra 4, 5 and 6, respectively). These are consistent with the corresponding pure mineral spectra shown in Figure 1. The associated alpha emissivity and MIRAC0$_2$LAS reflectance spectra (Figures 3b 'and 3c, respectively) also show similarities. However, the alpha emissivity spectra have a tilt towards shorter wavelengths which is not seen in the field μFTIR or MIRAC0$_2$LAS data and is caused by a processing artifact (Kealy and Hook, 1993). Narrow features (<0.2 μm) are not apparent in the TIMS spectra due to the resolution of the instrument but are clearly seen in the higher resolution MIRAC0$_2$LAS data, e.g. the dolomite trough centered at 11.2 μm and the tremolite features at 9.7 and 10.8 μm. Also the MIRACO$_2$LAS spectra have similar overall shapes to the field μFTIR spectra (Figure 3a) including high, relatively flat emissivities for the tremolite and dolomite spectra (Spectra 5 and 6 in Figure 3c). In addition, the MIRAC0$_2$LAS spectra show the diagnostic narrow spectral features at 9.7 and 10.8 μm for tremolite and 11.2 μm for dolomite. Spectrum 5 shows features associated with both minerals which indicates that minerals within mixtures can also be identified with the higher spectral resolution data. However, the limited wavelength range of MIRAC0$_2$LAS results in only a part of the dolomite 11.2 μm feature being resolved. A more complete wavelength coverage would be an advantage, particularly if other minerals are present, such as calcite which has a feature at 11.4 μm, outside

the MIRAC0$_2$LAS tuning range.

In the context of mineral exploration, it was possible to map two types of alteration within the upper part of the Balcanoona Formation, namely: talc-tremolite; and chlorite-gossan. Both of these types of alteration occur as various blue tones in the TIMS imagery (Figure 2) though it is not possible to identify the precise mineralogy. The higher spectral resolution of MIRACO$_2$LAS does allow for definitive mineral identification of the mineralogy. However, MIRACO$_2$LAS only collects data in line profile mode and so imaging, which is critical for target definition, is difficult. Improved geological mapping and mineral exploration should be expected from TIR systems capable of both measuring and imaging surface radiance at high spectral resolution (<0.2 μm) for the atmospheric window between 8 and 12 μm.

Conclusions

Airborne TIMS and MIRACO$_2$LAS data, as well as field μFTIR data, were acquired from the Mount Fitton area, South Australia to evaluate the role of these systems for geological mapping and mineral exploration.

It was possible to discriminate the major geological units with the TIMS imagery (Balcanoona, Mount Curtis Tillite, Amberoona and Nuccalena Formations) though precise mineral identification was generally not possible. This is because many of the diagnostic spectral features are much narrower than the TIMS bandpasses. Using MIRACO$_2$LAS enabled identification of the mineralogy of specific units as opposed to discrimination of these units in

Reference herein to any specific commercial product, process, or service by trade names, trademark, manufacturer or otherwise does not imply endorsement by the United States or the Jet Propulsion Laboratory, California Institute of Technology.

the TIMS imagery. Minerals that could be identified from the MIRAC0$_2$LAS included talc, quartz, tremolite and dolomite. The presence of these minerals was confirmed by geological mapping and field spectroscopy with the μFTIR. It is clear that an ideal remote TIR system for geological mapping and mineral exploration should comprise high spectral resolution (<0.2 μm wide bands) for the complete 8-12 μm atmospheric window and be able to generate images. These results suggest that, while such an instrument is not available, an instrument which includes a broad band imaging spectrometer and a high resolution profiling spectrometer would be far more valuable for geological studies than either instrument in isolation, since it would be possible to discriminate a geological unit in the image and then identify its mineralogy from a corresponding high resolution spectrum.

Acknowledgments

The research described in this paper was carried out in part at the Jet Propulsion Laboratory, California Institute of Technology, under a contract with the National Aeronautics and Space Administration as part of the Earth Observing System Mission to Planet Earth Program,

The joint TIMS/MIRACO$_2$LAS deployment in June 1993 was supported by NASA, CSIRO Division of Exploration and Mining and the CSIRO Office of Space Science and Applications. We acknowledge the engineering support of Duane O'Neill, Richard Phillips and Phil Connor and the software development by Peter Mason. Special thanks go to Commercial Minerals for providing access to the Mt Fitton site and also to Simon Powell for providing an overview of the geology.

References

Abrams, M. J., Abbott, E, A., and Kahle, A. B., 1991. Combined Use of Visible, Reflected Infrared and Thermal Infrared Images for Mapping Hawaiian Lava Flows. *Journal of Geophysical Research,* vol. *96,* pp. 475-484.

Berk, A., Bernstein, L. S., and Robertson, D, C., 1989. MODTRAN: A Moderate Resolution Model for LOWTRAN 7. *Tech. Rep. GL-TR-89-0122,* Geophys. Lab., Bedford, Mass.

Coats, R.P, and Blisset, A. H., 1971. Regional and economic geology of the Mount Painter Province. Bulletin Geological Survey of South Australia, 43,425 pages.

Crowley, J.K. and Hook, S. J., 1996. Mapping Playa Evaporite Minerals and Associated Sediments in Death Valley, California, with Multispectral Thermal Infrared Images. *Journal of Geophysical Research, vol.* 101, pp. 643-660.

Cudahy, T. J., Connor, P.M., Hausknecht, P., Hook, S.J., Huntington, J. F., Kahle, A. B., Phillips, R.N. and Whitbourn, L.B., 1994A: Airborne CO_2 Laser Spectrometer and TIMS TIR Data for Mineral Mapping in Australia, Proceedings of the 7th Australasian Remote Sensing Conference, Melbourne, pp. 918-924.

Cudahy, T. J., Whitbourn, L. B., Connor, P. M., Huntington, J. F., Mason, P. and Phillips, R. N., 1994B: Reduction of CSIRO Airborne $C0_2$ Laser (MIRACO_2LAS) Data to Ground

Reflectance. Exploration and Mining Report 59F,56 pages.

Eberhardt, J,E., Haub, J.G. andWhitbourn, L.B., 1988. Carbon Dioxide LaserTuningThrough llOLines in3msfor Airborne Remote Sensing. *Applied Optics*, vol. 27, pp. 879-884.

Gillespie, A.R., Kahle, A.B., and Palluconi, F.D., l984. Mapping Alluvial Fansin Death Valley, California using Multichannel Thermal Infrared Images. *Geophysical Research Letters,* vol. 11, pp. 1153-1156.

Gillespie, A. R., Kahle, A.B. and Walker, R. E., 1986. Color Enhancement of Highly Correlated Images. I. DeCorrelation and *HSI* Contrast Stretches. *Remote Sensing Environment,* vol. 20, pp. 209-235.

Hausknecht, P., Whitboum, L.B. and Connor, P. M., 1993: Rapid-Tuned 9-11 μm $C0_2$ Laser Remote Sensing System for Mineral Exploration, Proceedings of the 7th Conference on Coherent Laser Radar Applications and Technology, Paris, France, pp. 261-265.

Hook, S. J., Gabell, A. R., Green, A. A., and Kealy, P. S., 1992. A Comparison of Techniques for Extracting Emissivity Information from Thermal Infrared Data for Geologic Studies, *Remote Sens. Environ.,* vol. 42, pp. 123-135.

Hook, S. J., Karlstrom, K. E., Miller, C. F., and McCaffrey, K. J. W., 1994. Mapping the Piute Mountains, California, with Thermal Infrared Multispectral Scanner (TIMS) images.

Journal of Geophysical Research, vol. 99, pp. 15,605-15,622.

Hook, S.J. and Kahle, A. B., 1996, The micro Fourier Transform Interferometer (μFTIR) - A New Field Spectrometer for Validation of Infrared Data. *Remote Sensing Environment,* vol. 56, pp. 172-181.

Hunt, G. R., 1980. Electromagnetic Radiation: The communication link in remote sensing, in *Remote Sensing in Geology,* pp. 5-45, edited by B.S. Siegal and A. R. Gillespie, John Wiley and Sons, New York.

Kahle, A.B. and Goetz, A.F.H., 1983. Mineralogic Information from a New Airborne Thermal Infrared Multispectral Scanner. *Science,* vol. 222, pp. 24-27.

Kahle, A. B., Shumate, M.S. and Nash, D. B., 1984. Active Airborne Infrared Laser System for Identification of Surface Rock and Minerals. *Geophysical Research Letters,* vol. 11, pp 1149-1152.

Kealy, P. S., and Hook, S. J., 1993. Separating temperature and emissivity in thermal infrared multispectral scanner data: Implications for recovering land surface temperatures, *Geosci. Remote Sens.*, Vol. 31, pp. 1155-1164.

Lang, H. R., Adams, S. L., Conel, J. E., McGuffie, B. A., Paylor, E. D., and Walker, R. E., 1987. Multispectral Remote Sensing as Stratigraphic and Structural Tool, Wind River Basin

and Big Horn Basin Areas, Wyoming. *The American Association of Petroleum Geologists Bulletin,* vol. 71, pp. 389-403.

Lahren, M. M., Schweickert, R. A., and Taranik, J. V., 1988. Analysis of the northern Sierra accreted terrain, California, with airborne thermal infrared multispectral scanner data. *Geology,* vol. 16, pp. 525-528.

Liese, H. C., 1975. Selected terrestrial minerals and their infrared absorption spectral data (4000-300 cm- 1): in *Infrared and Raman Spectroscopy of Lunar and Terrestrial Minerals, C.* Karr, cd., Academic Press, New York, pp. 197-229.

Lyon, R, J. P., and Green, A.A. 1975. Reflectance and emittance of terrain in the mid-infrared (6-25 μm) region: in *Infrared and Raman Spectroscopy of Lunar and Terrestrial Minerals,* C. Karr, cd., Academic Press, New York, pp. 165-195.

Palluconi, F. D., and Meeks, G.R. Thermal infrared multispectral scanner (TIMS): An investigator's guide to TIMS data, *JPL Publ., 85-32,* 1985.

Sabine, C, Realmuto, V.J. and Taranik, J, V., 1994. Semiquantitative measurement of granitoid composition from thermal infrared multispectral scanner (TIMS) data, Desolation Wilderness, Northern Sierra Nevada, California. *Journal Geophysical Research,* vol. 99 pp. 4261-4271.

Siegal, R. and Howell, J. R., 1982. Thermal Radiation Heat Transfer: Second Edition. *Hemisphere Publishing Corporation, New* York,

Soha, J.M. and Schwartz, A, A., 1978. Multispectral Histogram Normalization Contrast Enhancement. *Proceedings of the Fifth Canadian Symposium on Remote Sensing,* Victoria, British Columbia, Canada, pp. 86-93.

Sprigg, R. C., 1951. Regional geology in the Mount Fitton talc area. In Dickinson, S. B., *et al.,* Talc deposits in South Australia. Bulletin Geological Survey of South Australia, 26, pp. 76-84.

Stillwell, F.L., and Edwards, A.B., 1951. Petrology of the Mount Fitton talc deposits. In Dickinson, S. B., *et al.,* Talc deposits in South Australia. Bulletin Geological Survey of South Australia, 26, pp. 101-108.

van der Mare], H. W., and Beutelspacher, H., 1976. Atlas of Infrared Spectroscopy of Clay Minerals and their admixtures. Elsevier Scientific Publishing Company, New York, 376p.

Watson, K. 1985. Remote sensing - A geophysical perspective. *Geophysics,* vol. 50, pp. 2595-2610.

Watson, K., Rowan, L. C., Bowers, T. L., Anton-Pacheco, C., Gumiel, P. and Miller, S. H., 1996.

Lithologic analysis from multispectral thermal infrared data of the alkalic rock complex at Iron Hill, Colorado. Geophysics, vol. 61, pp. 706-721.

Whitbourn, L, B., Phillips, R.N., James, G. and O'Brien, M.T., 1990. An airborne multiline CO_2 laser system for remote sensing of minerals. *J. Modem Optics, vol. 37,* pp. 1865-1872.

Whitbourn, L. B., 1991: 100 Wavelength Rapid-Tuned $C0_2$ Laser System Applied to Airborne Remote Sensing of Minerals, Proceedings of the International Conference on Lasers '91, San Diego, California, pp. 340-347,

Whitbourn, L. B., Hausknecht, P., Huntington, J.F. Connor, P. M., Cudahy, T. J.and Phillips, R. N., 1994: Airborne $C0_2$ Laser Remote Sensing System. Proceedings of the 1st International Airborne Remote Sensing Conference and Exhibition: Applications, Technology and Science, Strasbourg, France, September 12-15, pp. II-94 - II-103.

Figures

Figure 1. Left panel: Hemispherical reflectance spectra converted to emissivity using Kirchhoff's Law for a variety of minerals, measured using the Jet Propulsion Laboratory Nicolet 520 Interferometer spectrometer with a hemispherical attachment. Right panel: Bi-directional reflectance spectra converted to emissivity using Kirchhoff's Law for a variety of minerals measured using the CSIRO Laboratory $C0_2$ laser spectrometer. Both panels: Ta - Talc, Qu - Quartz, Al - Albite, Mi - Microcline, Mu - Muscovite, Tr - Tremolite, Do - Dolomite, Ma - Magnesite.

Figure 2. TIMS decorrelation stretch image (left) and corresponding geological map (right) over the study area with the positions of the MIRACO_2LAS flight lines superimposed as white lines. The TIMS image was created by performing a decorrelation stretch on the radiance data from channels 5, 3 and 1 then displaying the result in red, green and blue respectively. The image was also panoramically corrected. Geological map of the area covered by the image redrawn from the 1:25,000 Geological Map of the Mount Painter Province. Labels indicate sites discussed in the text. Number labels refer to sites from which spectra were obtained for Figures 3a-c. Letter labels refer to sites discussed in the text.

Figure 3a. Field emissivity spectra derived with the micro Fourier Transform Interferometer (μFTIR) data for the six sites labeled on Figure 2. Spectra are offset for clarity. The emissivity value at 12 μm is labeled on the right hand side of the plot. See Hook and

Kahle, (1996) for a discussion of the reduction of the μFTIR data,

Figure 3b. Alpha emissivity spectra derived from the TIMS data from six sites labeled on Figure 2. Spectra are offset for clarity. The alpha residual value in TIMS channel 6 is labeled on the right hand side of the plot. See Kealy and Hook (1993) for a discussion of the reduction of TIMS data to alpha residuals,

Figure 3c. Emissivity spectra derived from MIRACO$_2$LAS data for the six sites labeled on Figure 2. Spectra are offset for clarity. The emissivity value for the final laser line is labeled on the right hand side of the plot.

Laboratory Data

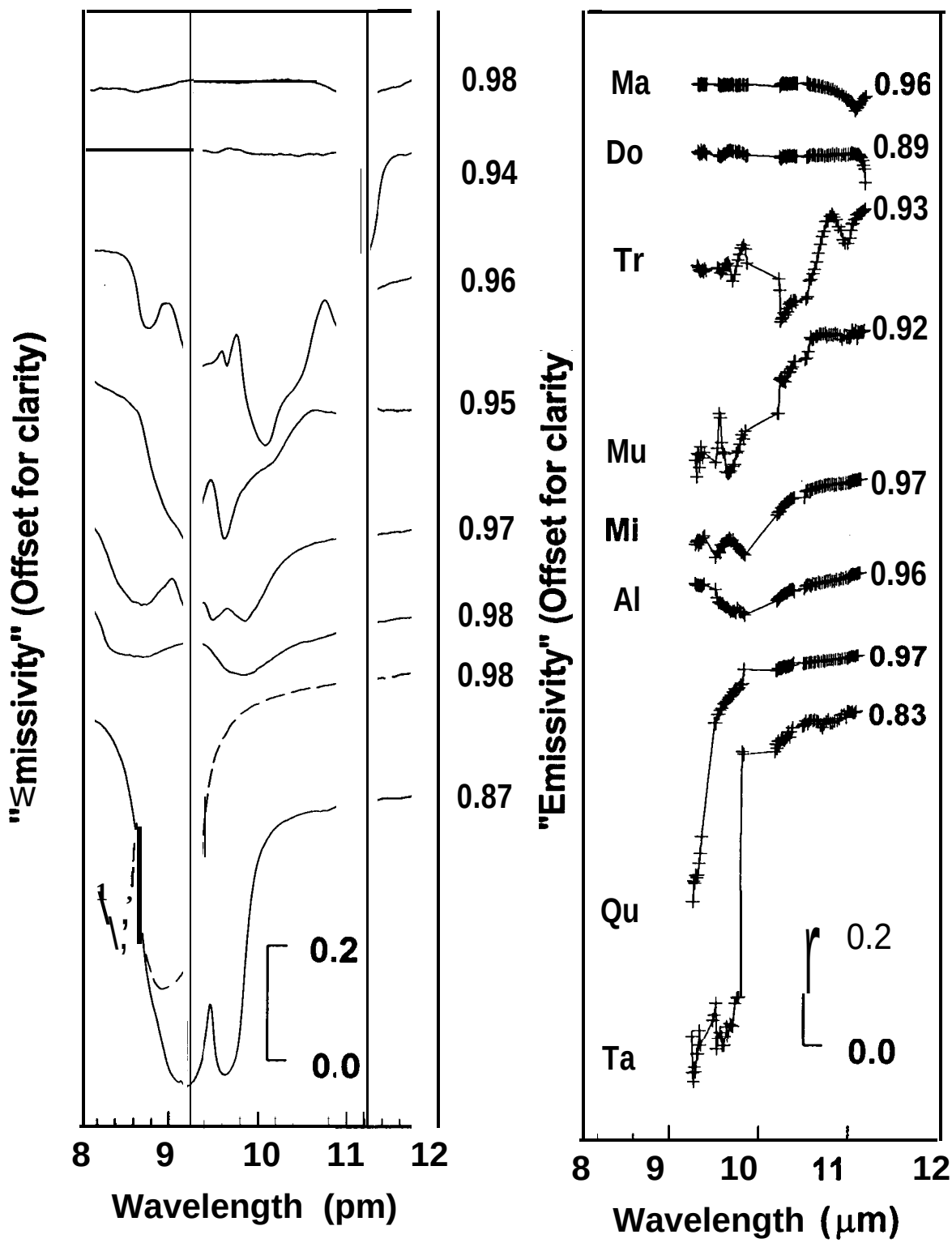

Hook et al Figure 1.

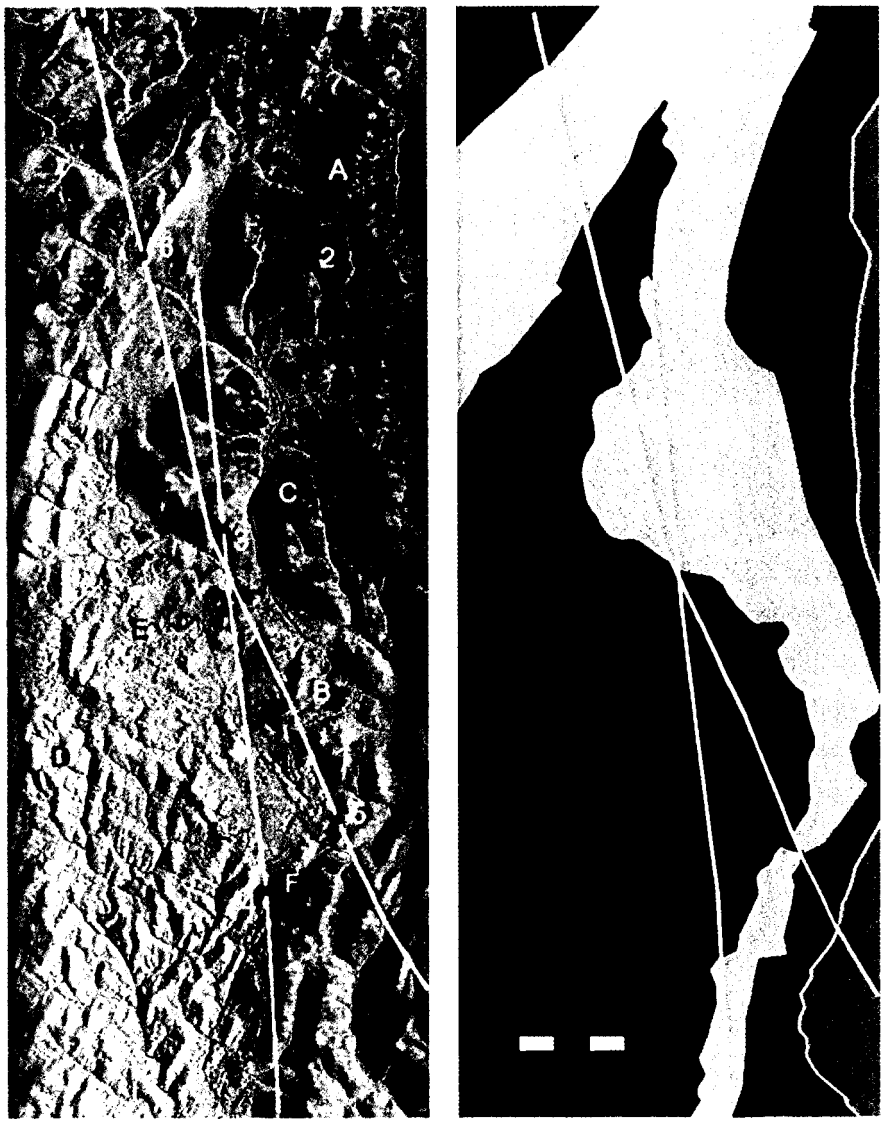

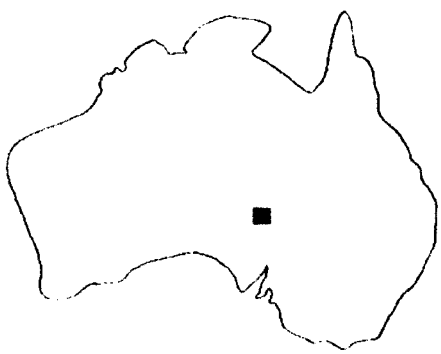

Legend

Nuccaleena Formation

Mt Curtiss Tillite Formation

Amberoona Formation

Balcanoona Formation

Hoda et al Figure 2

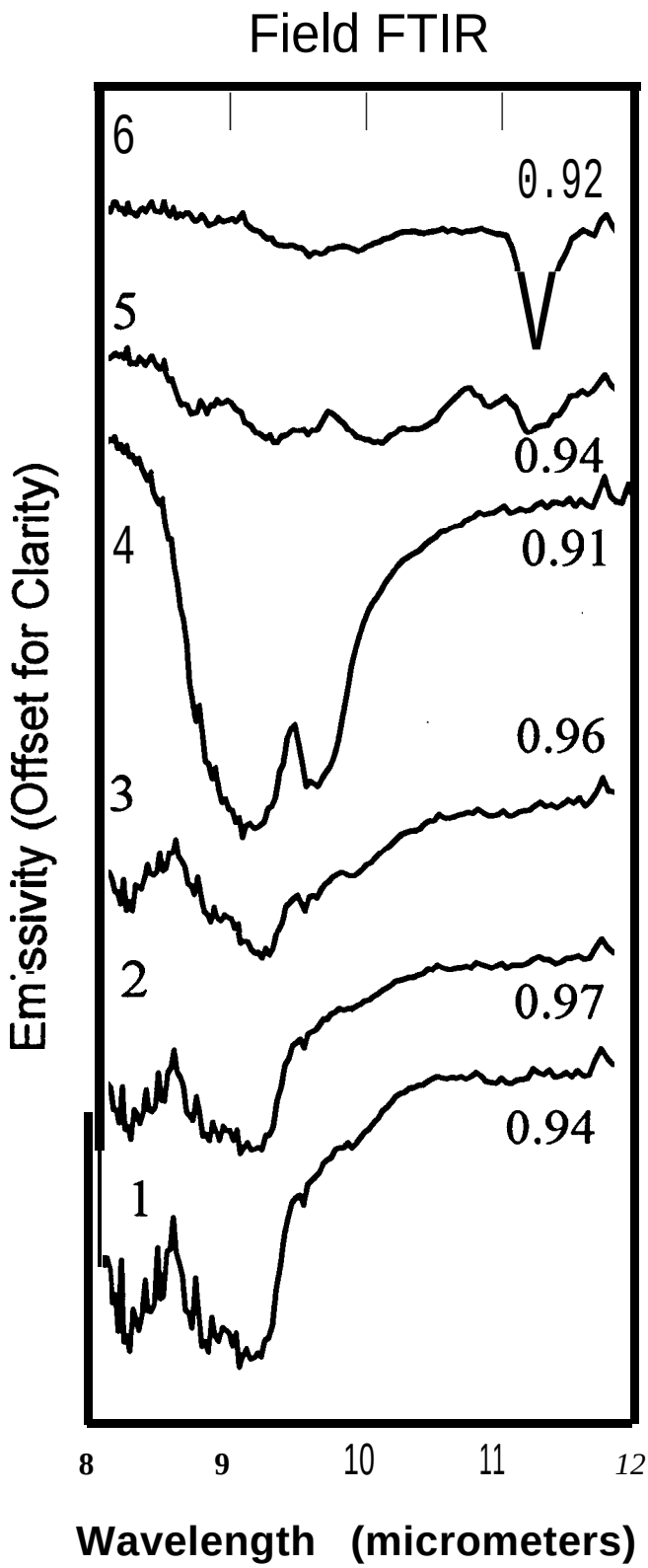

Hook et al Figure 3a

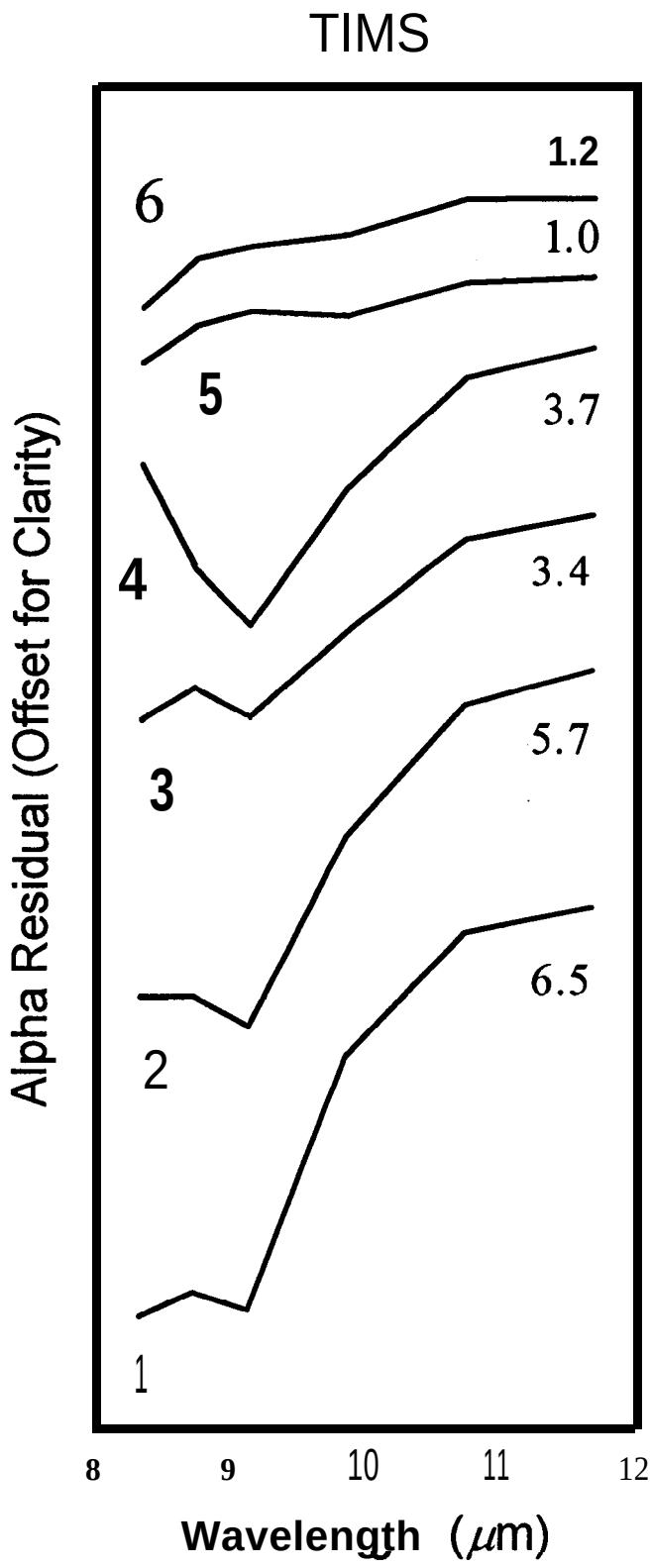

Hook et al. Figure 3b

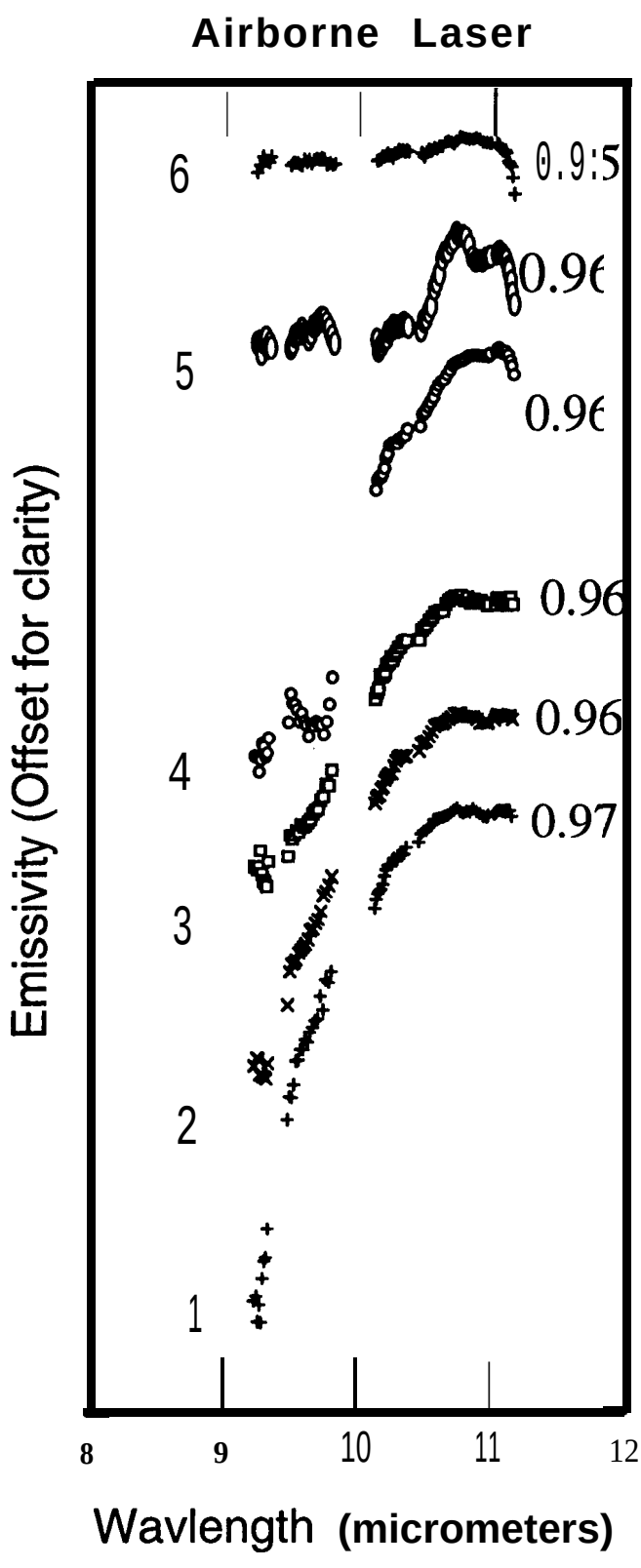

Hook et al Figure 3c